ADVANCED OPTICAL MATERIALS
www.advopticalmat.de

Strong Induced Circular Dichroism in a Hybrid Lead-Halide Semiconductor Using Chiral Amino Acids for Crystallite Surface Functionalization

*Markus W. Heindl, Tim Kodalle, Natalie Fehn, Lennart K. Reb, Shangpu Liu, Constantin Harder, Maged Abdelsamie, Lissa Eyre, Ian D. Sharp, Stephan V. Roth, Peter Müller-Buschbaum, Aras Kartouzian, Carolin M. Sutter-Fella, and Felix Deschler**

Chirality is a desired property in functional semiconductors for optoelectronic, catalytic, and spintronic applications. Here, introducing enantiomerically-pure 3-aminobutyric acid (3-ABA) into thin films of the 1D semiconductor dimethylammonium lead iodide ($DMAPbI_3$) is found to result in strong circular dichroism (CD) in the optical absorption. X-ray diffraction and grazing incidence small angle X-ray scattering (GISAXS) are applied to gain molecular-scale insights into the chirality transfer mechanism, which is attributed to a chiral surface modification of $DMAPbI_3$ crystallites. This study demonstrates that the CD signal strength can be controlled by the amino-acid content relative to the crystallite surface area. The CD intensity is tuned by the composition of the precursor solution and the spin-coating time, thereby achieving anisotropy factors (g_{abs}) as high as 1.75×10^{-2}. Grazing incidence wide angle scattering reveals strong preferential ordering that can be suppressed via tailored synthesis conditions. Different contributions to the chiroptical properties are resolved by a detailed analysis of the CD signal utilizing an approach based on the Mueller matrix model. This report of a novel class of chiral hybrid semiconductors with precise control over their optical activity presents a promising approach for the design of circularly polarized light detectors and emitters.

1. Introduction

Chirality is a fundamental property in chemistry that occurs, for example, when two variants of a molecule exist that appear as mirrored images of each other but cannot be superimposed. While the general chemical behavior of these so-called enantiomers is similar, their reactivities may vary significantly when interacting with other chiral systems. As a consequence, chirality has been a key property for biochemical applications.[1] Increasingly, chiral compounds are also studied for their optical and electronic properties, manifested for instance as circular dichroism (CD), in which there is preferred absorption of left or right hand circularly polarized light, or circularly polarized luminescence.[2–4] A promising approach to exploit these traits for technological applications is the combination of chiral organics with hybrid lead-halide perovskites,[5–7] whose extraordinary

M. W. Heindl, S. Liu, L. Eyre, I. D. Sharp, F. Deschler[+]
Walter Schottky Institut and Department of Physics
Technical University of Munich
Am Coulombwall 4, 85748 Garching, Germany
E-mail: deschler@uni-heidelberg.de

T. Kodalle, C. M. Sutter-Fella
Lawrence Berkeley National Laboratory
1 Cyclotron Rd., Berkeley, CA 94720, USA

The ORCID identification number(s) for the author(s) of this article can be found under https://doi.org/10.1002/adom.202200204.

[+]Present address: Physikalisch-Chemisches Institut, Universität Heidelberg, Im Neuenheimer Feld 229, 69120 Heidelberg

DOI: 10.1002/adom.202200204

N. Fehn, A. Kartouzian
Catalysis Research Center and Chemistry Department
Technical University of Munich
Lichtenbergstraße 4, 85748 Garching, Germany

L. K. Reb, C. Harder, P. Müller-Buschbaum
Physik-Department
Technische Universität München
James-Franck-Straße 1, 85748 Garching, Germany

C. Harder, S. V. Roth
Deutsches Elektronen-Synchrotron (DESY)
Notkestr. 85, 22607 Hamburg, Germany

M. Abdelsamie
Materials Sciences Division
Lawrence Berkeley National Laboratory
1 Cyclotron Rd., Berkeley, CA 94720, USA

S. V. Roth
KTH Royal Institute of Technology
Teknikringen 56–58, Stockholm 10044, Sweden

P. Müller-Buschbaum
Technische Universität München
Lichtenbergstr. 1, 85748 Garching, Germany

chemical versatility allows for the incorporation of the small molecules into their inorganic lattice. This results in chirality transfer effects, in which the organic molecule imprints chiral properties onto the previously achiral inorganic lattice, either via an (intramolecular) chemical bond or due to proximity effects.[8–10] Such approach has enabled a number of promising results on the spin-selective transport of charge carriers,[11–13] ferroelectric performance,[14,15] and the generation and detection of circularly polarized light.[6,7,16–19] An alternative method of obtaining chiral perovskite materials is via surface functionalization of nanocrystals, where research has mostly focused on the outstanding chiroptical properties that can be obtained.[20–23] Despite these promising demonstrations, research has thus far been limited to only a handful of chiral molecules,[9,24] which are almost exclusively made up of amides with an aryl or alkyl moiety. However, studies devoted to halide substitution have already shown that small changes to these chiral compounds can have a dramatic impact on the optoelectronic performance of semiconductors.[15,25–27] Hence, expanding the pool of chiral organics for perovskite functionalization is desirable for developing new applications and optimizing existing ones.

In the present work, we explore the use of alternative biomolecular candidates as the chiral component of hybrid semiconductors. In particular, we aim to leverage the abundance of chiral compounds in biological systems, such as those comprising DNA, carbohydrates, and volatile organic compounds usually associated with taste or smell.[1,28] We focus on amino acids, since they represent a chemically diverse group of small, chiral molecules with a range of functional groups. Furthermore, the vast majority of these compounds display no health risks and many enantiomerically pure compounds are readily available in large quantities at relatively low cost. A first attempt has been made recently when Sirenko et al. incorporated α-alanine into a 2D hybrid perovskite. However, no chirality transfer effects were reported.[29]

In this work, we report and analyze the occurrence of chirality transfer effects between dimethylammonium lead iodide ($DMAPI_3$) and the β-amino acid 3-aminobutyric acid (3-ABA), which is a signaling molecule in plants.[30] We discuss synthesis strategies for solution-processed thin films and optimize fabrication conditions to maximize the CD signal for absorption in the blue and UV spectral regions. Using X-ray diffraction (XRD) and grazing incidence small angle X-ray scattering (GISAXS), we elucidate the detailed origin of the chirality transfer mechanism. Further, we show that a Mueller-matrix-based approach is required to optimize chiroptical effects in chiral hybrid perovskite materials since unwanted non-chiral contributions to the CD signal may obscure intrinsic CD effects. To the best of our knowledge this represents the first proof of chirality transfer between an amino acid and a lead halide semiconductor thin film, which demonstrates the promise of similar, biological molecules for the discovery of chiral hybrid semiconductors. Furthermore, we propose a novel approach for imprinting chiral properties onto previously achiral solid thin films, which is based on the surface modification of the individual crystallites with chiral ligands. This allows for chirality transfer effects similar to those observed for colloidal nanocrystals.

2. Results and Discussion

We use $DMAPbI_3$ as the base material for functionalization with amino acids, since it allows for easy solution-based processing and possesses a prototype 1D structure of face-sharing $[PbI_6]$ octahedra that form continuous chains. These are surrounded by DMA^+-cations which supply the missing positive charge, as shown by the graphic representation in Figure S1, Supporting Information. We note that, because of its ABX_3 formula and octahedra-based structure, this compound is often referred to as a 1D perovskite, even though it does not display the corner-sharing motif typically required to define the perovskite structure.[31,32] We prepare the material by spin-coating a dimethyl sulfoxide (DMSO) solution containing 0.5 mol L^{-1} PbI_2 and 0.55 mol L^{-1} DMAI on a glass substrate for 20 s, followed by annealing for 30 min at 60 °C (for details see Experimental Section). To achieve chiral thin films, this synthesis process was repeated under the same conditions, but with 0.5 mol L^{-1} of (*R*)-3-ABA or (*S*)-3-ABA (see **Figure 1**a) added into the precursor solution.

In order to investigate whether any interactions take place between the hybrid semiconductor and the amino acid, the optical properties of the synthesized materials were studied using absorption and CD spectroscopy (Figure 1b,c), which probes preferential absorption of one form of circularly polarized light. Pure $DMAPbI_3$ displays a first excitonic absorption peak at ≈380 nm and no measurable CD signal is observed, which is expected given the achiral P63/mmc space group reported for $DMAPbI_3$.[9,31] Importantly, the absorption spectrum of the (*R*)-3-ABA containing $DMAPbI_3$ composite is qualitatively similar to its achiral counterpart, though the first excitonic peak is slightly blue shifted and the overall absorbance is significantly stronger. The CD spectrum of this material, as seen in Figure 1, displays three distinct peaks at ≈330, ≈380, and ≈405 nm in the blue and UV spectral regions, as well as a long tail from about 450 to 550 nm due to scattering effects. Another potential peak at ≈300 nm is cut off by the absorption of the glass substrate. The steep zero-crossing at ≈390 nm thereby may be indicative of a Cotton effect relating to the excitonic transition at ≈380 nm. Since this zero crossing does not match the absorption maximum exactly and the integral of the lower energy part of the signal appears more intense than the high energy one, an additional contribution has to be considered. This could be attributed to a small shoulder at ≈405 nm in the absorption spectrum, indicating an additional transition there. The other signals at ≈300 and ≈330 nm hence originate from transitions relating to higher energy bands.

The CD-signal of the corresponding (*S*)-enantiomer appears mirrored along the wavelength-axis (Figure S2, Supporting Information), providing strong evidence that the observed signal originates from chirality transfer effects. Alternatives, such as the formation of a rotation-induced chiral supramolecular structure introduced during spin-coating, as has for instance been reported for some J-aggregates, can hence be excluded, since the direction of rotation remained unchanged.[33] Further indication for molecular-level chirality within the thin film is provided by the fact that no CD effect is observed when introducing the corresponding racemate (*rac*)-3-ABA into the $DMAPbI_3$ thin film (Figure S3,

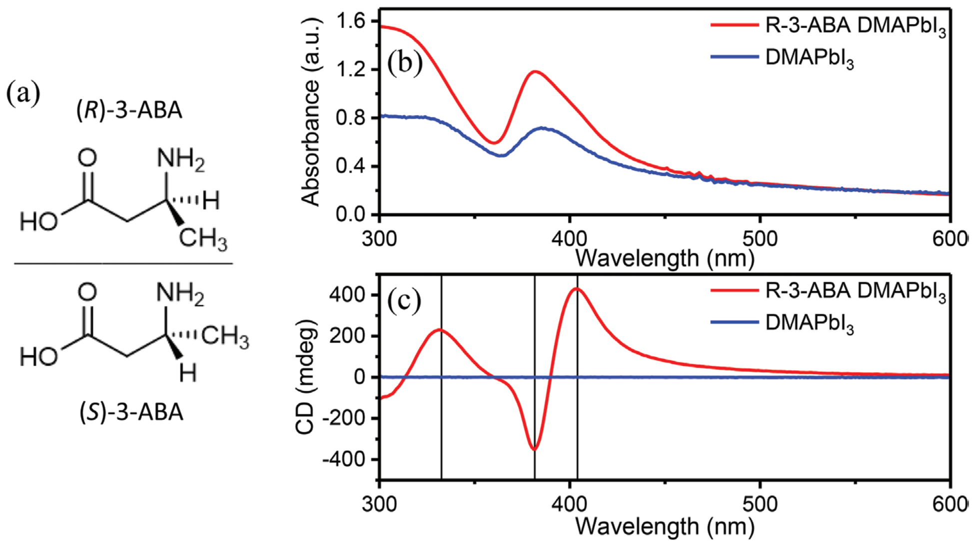

Figure 1. a) Molecular structure of (*R*)- and (*S*)-3-ABA and b,c) chiroptical properties of two $DMAPbI_3$ thin films, pure (blue) and with added (*R*)-3-ABA (1:1 PbI_2:(*R*)-3-ABA ratio, red). b) Absorption spectra of spin-coated thin films. Strong absorption in the blue and UV spectral regions is seen for both materials. c) Circular dichroism (CD) spectra for thin films of pristine $DMAPbI_3$ and (*R*)-3-ABA containing $DMAPbI_3$. CD signals are only observed in films containing the amino acid, which indicates chirality transfer between organic and inorganic components. The three distinct CD peaks at ≈330, ≈380, and ≈405 nm are marked with vertical lines.

Supporting Information). Since neither a lead-amino acid film nor the pure amino acid in solution display a strong CD signal in this spectral region (Figures S4 and S5a, Supporting Information), we conclude that this signal originates from the formerly non-chiral $DMAPbI_3$, indicating the occurrence of chirality transfer effects between the chiral amino acid and the hybrid semiconductor.

In order to investigate the structural origins of the CD signal, we probe the crystal structures of the films using X-ray diffraction (**Figure 2**). Pure $DMAPbI_3$ displays its prominent (100) peak at 11.6°, along with several less intense peaks above 15°. For the amino-acid containing samples we find an additional peak at 6.4°, with related higher order reflections at 12.8° and 19.2°. Reference measurements on the pure amino acid powder reveal that these signals do not correspond to the pure amino acid (see Figure S5b, Supporting Information). To probe changes of the crystal structure with depth, we measured grazing-incidence wide-angle X-ray scattering (GIWAXS) at different incident angles.[34] It is observed that the intensity of the 6.4° reflex decreases more rapidly with increasing incidence angle than the intensity of the (100) Bragg peak of pristine $DMAPbI_3$, indicating that the origin of this new diffraction signal is predominantly located at the surface of the thin film (Figure S6, Supporting Information). Possible origins of such a signal may be the formation of a crystalline amino acid-lead complex on the film surface or of the bifunctional amino acid acting as a spacer between two $DMAPbI_3$ unit cells, which may result in a complexly ordered structure with some degree of long range order.

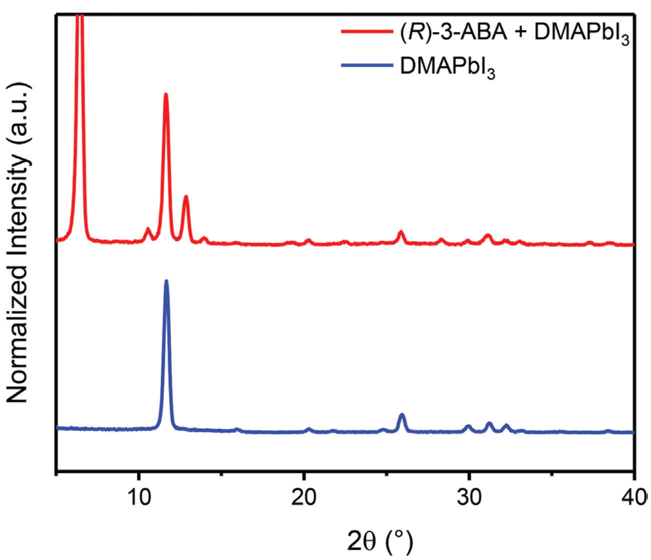

Figure 2. Structural properties of chiral hybrid lead-halide compounds with $DMAPbI_3$ motif. XRD patterns of (bottom, blue) a pure $DMAPbI_3$ thin film and (top, red) a (*R*)-3-ABA containing $DMAPbI_3$ thin film. The original $DMAPbI_3$ structure is preserved upon adding the amino acid.

We also note two additional peaks at 10.6° and 13.9°, which will be discussed below. Remarkably, all $DMAPbI_3$ reflections also occur for the (*R*/*S*)-3-ABA containing films, which is an indication that the original structure of 1D chains is preserved. This finding agrees with the absorption data, which matches the original absorption spectrum of pure $DMAPbI_3$ in its peak position. Since an introduction of the zwitterionic amino acid into the lattice would also change the crystal structure, this would also alter the XRD patterns and most likely the absorption wavelength, which is not the case (see Figure 1). Thus, we conclude that no new bulk chiral crystal phase is formed upon the introduction of the amino acid. Instead, we propose that the origin of the CD arises from a chirality transfer to the $DMAPbI_3$ lattice via surface interactions. Since the amino acid is a zwitterionic species, chemical bonds with the surface can occur via the positive charge possessed by the protonated amino group or the negative charge from the deprotonated carboxyl group. Using a beta- instead of an alpha-amino acid results in additional spatial separation of the two charges and, hence, may allow both functional groups to interact with different surfaces species at the same time, leading to an overall stronger bond. In this chirality transfer mechanism, the amino acid interacts with the surfaces of the nanometer-scaled $DMAPbI_3$ crystals—generally referred to as crystallites or grains—that comprise the thin film. An example for such a mechanism is chiral surface distortion, an effect well known from chiral nanocrystals.[9,20,21] Similarly, chirality transfer effects between transition-metal nanostructures and surface-bound amino acids have been described repeatedly.[35,36] Establishing this mechanism for the use in spin-coated materials provides a new method for obtaining high-quality in thin films with chiral properties.

To test the hypothesis that surface chirality transfer gives rise to the observed CD, we investigated the impact of film morphology on chiroptical properties by varying the fabrication conditions. To this end, we increased the spin-coating time from 20 to 100 s. This results in significantly larger average crystallite sizes for the 100 s sample (**Figure 3**a), as resolved by GISAXS. This technique allows for statistically relevant sampling of the lateral morphology on the nanometer-scale throughout the entire depth of the thin film—unlike surface-focused scanning electron microscopy (SEM)—by modeling the form factor distribution from the obtained data (Figure S7, Supporting Information).[37] Importantly, the resulting CD signal is weaker for the 100 s spin-coated film than for the 20 s one, while the primary structure of three signal peaks is preserved (Figure 3b, top). This supports the idea of a chirality transfer phenomenon based on interactions on the $DMAPbI_3$-crystallite surfaces, since the observed reduction in the surface to bulk ratio for the 100 s sample would explain the decrease in CD-intensity. Based on this observation, films with smaller grains would be beneficial for obtaining strong CD signals. This would require maximizing the nucleation rate while suppressing grain coarsening. Available options to achieve this include optimizing the choice of precursor concentration, solvent (mixture), spin-coating time and speed, as well as the annealing temperature of the still wet film. Another possibility could be the well-timed addition of an antisolvent, which has been shown to greatly influence the nucleation and crystallization process during spin-coating.[38]

Prolonging the spin-coating time also results in the disappearance of the peaks at 10.6° and 13.9° (Figure S8, Supporting Information), indicating that this unknown impurity phase can be removed by changing the reaction conditions. It also results in a much smoother film surface, as revealed by SEM imaging (Figure S9, Supporting Information). Furthermore, no significant difference between the two samples is observed in absorption spectroscopy, indicating that these impurities do not contribute to the optoelectronic properties described so far (Figure 3b, bottom). The observed decrease in scattering by the sample spin-coated for 100 s can thereby be explained by the smoother film surface mentioned above.

In order to probe the film formation processes that define the nanoscale morphology, and thus the surface chirality transfer, we performed in-situ optical absorption spectroscopy during the spin-coating process. As shown in **Figure 4**, the absorption spectrum evolves to its final form over a period of ≈80 s during spin-coating. Thus, for the case of the 100 s spin-coating process, the absorption spectrum is fully formed by the time the rotation comes to an end (Figure 4a). In contrast, for the 20 s spin-coated sample the final optical properties of the film are only established during the subsequent drying step (Figure 4b). This observation reveals that the structures and properties of the two different films are defined under vastly different reaction conditions. As discussed above, from the standpoint of film synthesis optimization, processes that increase the nucleation rate, minimize grain size, and suppress coarsening are expected to promote surface chirality transfer and increase

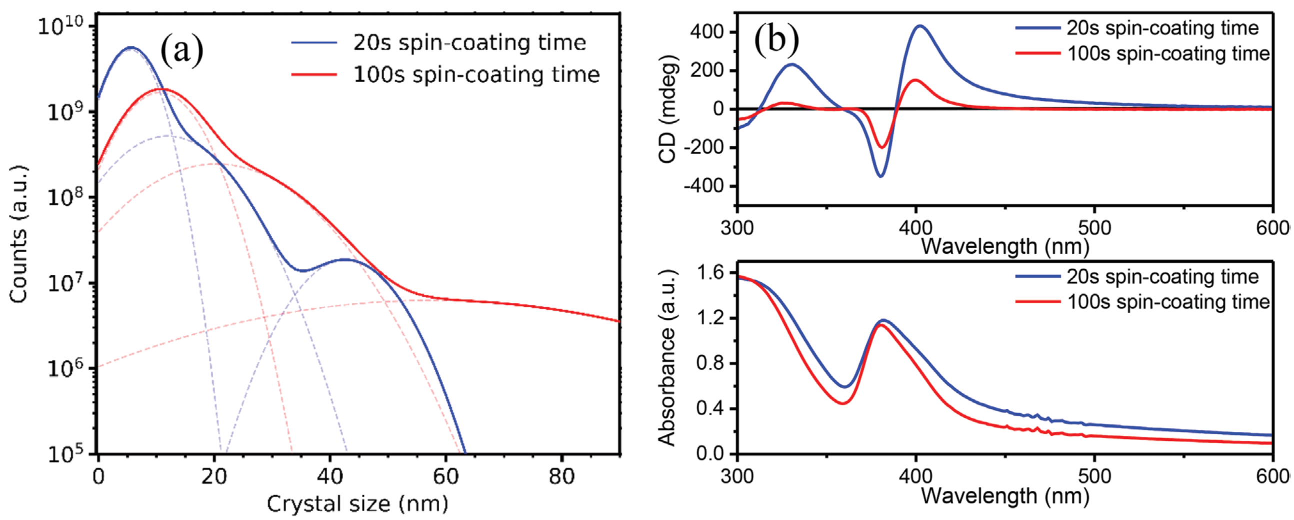

Figure 3. Influence of spin-coating time (20 s versus 100 s) on the formation of (*R*)-3-ABA containing $DMAPbI_3$ thin films. a) Form factor size distributions retrieved from modeling GISAXS data show three main crystal sizes. A longer spin-coating time leads to larger average radii for all three form factors. b) CD-signals decrease with longer spin-coating times, while the absorption intensity remains mostly unchanged, indicating a dependency between the size of crystallites and the CD intensity.

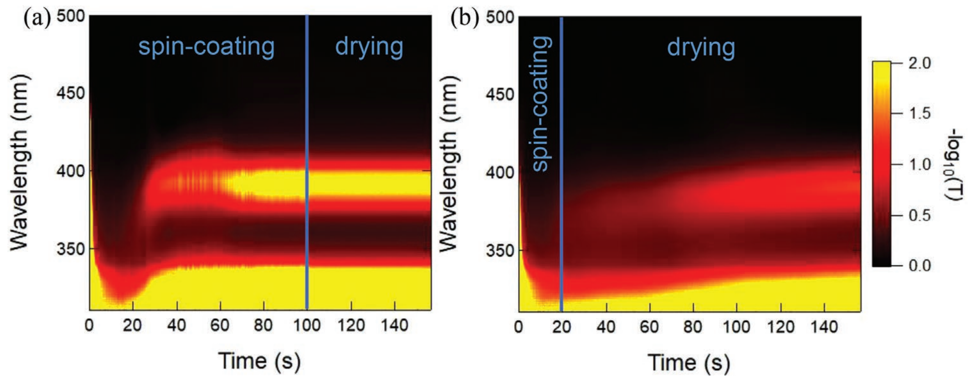

Figure 4. Temporal evolution of in situ UV–Vis absorption spectra during film formation. a) After spin-coating for 100 s, the absorption spectrum has fully evolved, indicating that the thin film formation including the solvent evaporation process has mostly been completed. b) When spin-coating for 20 s, film formation is still ongoing and is only completed during the subsequent drying step. We note that the used setup does not allow for heating.

the magnitude of CD. Likewise, the observed differences in temperature and presence of solvent molecules could affect the precursors' mobility during the film formation and hence influence the CD effect by altering the amount and orientation of the chiral component on the crystallites' surfaces.

To further understand the origins of the chirality transfer phenomenon we perform concentration-dependent CD measurements with varying amounts of (*S*)-3-ABA added to the precursor solution. We expect a change in CD intensity based on the availability of the chiral component on the surfaces of the crystallites. Since a different precursor chemistry could also affect the film thickness and hence the CD signal intensity, a comparison in the traditional unit (mdeg) may not be completely accurate. Therefore, the results are analyzed in the form of the anisotropy factor, g_{abs}, which is based on normalizing the difference in the absolute absorption values, as described in Equation (1):[9,39]

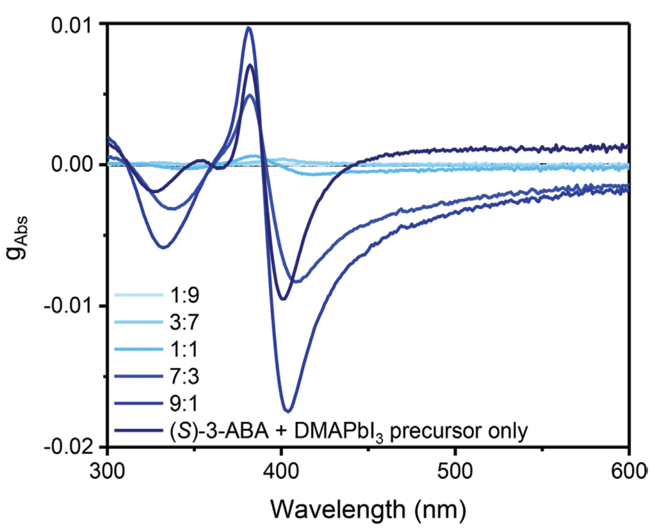

Figure 5. Control of chiroptical properties of (*S*)-3-ABA functionalized $DMAPbI_3$ via added amino acid content. The CD signal strength increases with increased amino acid content, exhibiting a maximum for a precursor solution ratio of 9:1 (*S*)-3-ABA/$DMAPbI_3$:$DMAPbI_3$. Compared to Figures 1 and 3, the CD signal appears mirrored along the wavelength-axis since here the (*S*)- rather than the (*R*)-enantiomer was used.

$$g_{abs} = \frac{2 \times (A_+ - A_-)}{A_+ + A_-} \tag{1}$$

with A_+ and A_- representing the absorption of right- and left-handed polarized light.

The (*S*)-3-ABA-concentration dependent CD signals can be seen in **Figure 5**, the corresponding absorption measurements in Figure S10, Supporting Information. The obtained data exhibit a non-linear connection between the amino acid to lead iodide ratio and the g_{abs}-value. For a low (*S*)-3-ABA-concentration (1:9 (*S*)-3-ABA/$DMAPbI_3$:$DMAPbI_3$ precursor solution mixing ratio), no CD signal is observed, and only weak signals can be detected for the 3:7 and 1:1 ratios. In agreement with theoretical models on perovskite clusters,[40] the signal intensity grows significantly, if the amino acid content is increased further. A maximum is reached between a 7:3 and a 9:1 ratio. The highest observed g_{abs}-value is 1.75×10^{-2}. Adding even more amino acid—by using the pure (*S*)-3-ABA/$DMAPbI_3$ precursor solution—decreases the CD intensity again. DFT calculations have shown that for multidentate ligands the CD effect is governed by the exact binding configuration of the organic.[40] This suggests that under excess of 3-ABA a higher surface coverage can be achieved, which hence decreases the CD intensity through partial differences in the binding geometry of the chiral component. Overall, this concentration dependence represents a facile and straightforward approach to adjust the CD intensity by controlling the amount of amino acid available for surface functionalization.

Finally, we used an approach developed by Shindo et al. and based on theoretical considerations set out by the Mueller matrix model to investigate the occurrence of other optical phenomena within the material, in particular linear dichroism (LD) and linear birefringence (LB). These can occur both individually as instrument-dependent artifacts and as a combined LDLB effect that emerges as a genuine signal if the main axes of both effects are misaligned.[41–43] Since these effects are not related to chiral phenomena but can nevertheless contribute to the measured electronic CD signal, they are able to distort the obtained results. This technique can be therefore be considered due diligence for any study on chiral thin films.[39,43] To apply this Mueller matrix-based approach, several CD spectra were recorded from the same sample, which was rotated and flipped between the measurements. Herein, LD and LB contributions are detectable upon changes in the CD signal when rotating the sample along the optical axis by 45°. Any influence of the LDLB term can be observed when flipping the sample (from the sample facing the detector to the substrate facing the detector).[44] For the 20 s spin-coated samples, all measurement orientations result in a very similar CD signal (Figure S11a, Supporting Information). Hence, neither LD, LB nor LDLB effects are observed to contribute significantly. Smaller deviations can be explained by the different reflectivity of glass and sample. For the samples spin-coated for 100 s, again no changes are observed upon rotation, suggesting an absence of LD and LB artifacts. However, the CD signal appears weaker when the glass is flipped to facing the light source (**Figure 6**), even though overall absorption stays the same (Figure S11b, Supporting Information). This indicates the presence of a different alignment of the LD and the LB main axis within the sample and hence an LDLB contribution to the combined CD signal.

Why this effect is observed for the sample spin-coated for 100 s but not the one spin-coated for 20 s cannot be explained in a straightforward manner since both LD and LB contributions, as well as their interplay, have to be taken into account. However, two potential contributions to this observation can be identified. One aspect to consider is that LB effects can be introduced through mechanical stress.[45] As we have established in Figure 4, crystallization in the sample spin-coated for 100 s takes place during spin-coating while strong shear-forces resulting from the rotation are applied to the material. This may constitute a key difference to the sample spin-coated for 20 s since here crystallization takes place only after rotation has concluded. Furthermore, since LDLB is a result of a misalignment in the main axes of both effects, the crystallite orientation is a key factor to consider.

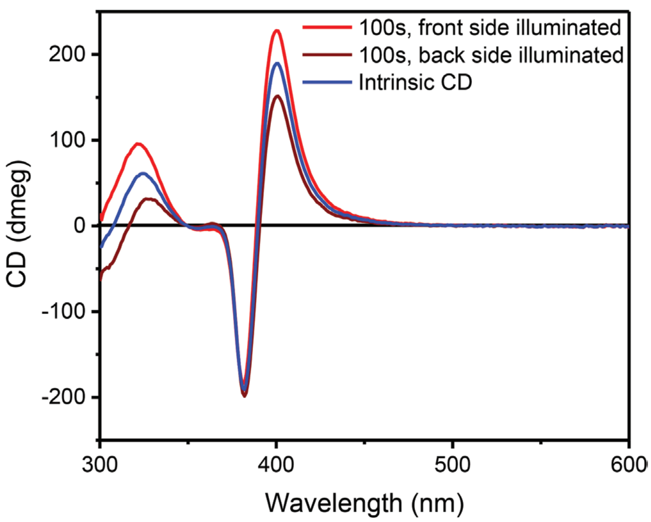

Figure 6. Selected measurements for (*R*)-3-ABA containing $DMAPbI_3$ films, spin-coated for 100 s. A difference in CD intensity is observed upon flipping the sample from the thin film facing the detector (bright red, front side illuminated) to the glass substrate facing the detector (dark red, back side illuminated), indicating LDLB contributions. The intrinsic CD intensity without contributions not relating to chiral effects is approximated by averaging both measurements (blue).

To investigate this aspect, we again applied GIWAXS. Here, the sample is probed with the focused X-ray beam above its critical angle. Thus, we obtain scattering data containing bulk-film information on the orientations of the crystallites.[46,47] The GIWAXS data display narrower and more defined intensity peaks for the sample spin-coated for 100 s than for the 20 s sample (Figure S12a–d, Supporting Information), a fact that becomes even more apparent when considering the azimuthal tube-cuts along the $DMAPbI_3$ (100) Bragg reflex (Figure S12e,f, Supporting Information). In these cuts the most intense signals at χ-angles of –60°, 0° and 60° appear narrower for the sample spin-coated for 100 s than for the one spin-coated for 20 s, already indicating a more defined orientation of the crystallites. To quantify the observed changes, we derive pole figures from the tube cuts that are representative for the amount of material contributing to a certain angle χ. We observe a strong isotopic signal for the 20 s sample, as well as intense but broadened central peaks and two symmetric side peaks centered at χ-angles of –60° and 60° with a smaller area than the central peaks (**Figure 7**a). In comparison, the pole figures for the sample spin-coated for 100 s (Figure 7b)—while still displaying a strong isotropic signal—show overall narrower peaks as well as a strong shift in area from the central to the side reflexes, which are about three times more pronounced than the central ones. These surprisingly strong changes between the two spin-coating times indicate a significant change in the preferential orientation of the crystallites, which is likely to influence the LDLB effect.

3. Conclusion

We report that the chiral amino acid (*S*/*R*)-3-ABA introduces CD effects in the absorption of the hybrid lead halide 1D-semiconductor $DMAPbI_3$. To the best of our knowledge this represents the first proof of successfully using an amino acid to introduce chirality into a lead-halide based thin film semiconductor. GISAXS and XRD data indicate that the chiral component is located on the surface of the $DMAPbI_3$ crystallites, allowing for chiroptical interactions and extensive control over the CD signal, especially when compared to 1D and 2D perovskites that incorporate fixed amounts of chiral organics into their crystal structure. We show that this tuning of the CD intensity can be achieved by adjusting the precursor composition and the spin-coating time. We furthermore note that, under optimized fabrication conditions, the observed anisotropy factor, g_{abs}, reported here exceeds that of (*R*/*S*)-MBA_2PbI_4—the perhaps most studied chiral 2D-perovskite—by one order of magnitude,[11] making it a promising candidate for the detection of circularly polarized light. Mueller-matrix-based analysis reveals non-chiral contributions to the CD spectrum upon increased spin-coating times, highlighting the need for including these effects in future optimization of chiral perovskite thin films. GIWAXS experiments reveal that this effect may, in part, originate from the introduction of a preferred orientation among the crystallites that can be suppressed by spin-coating for shorter times to yield more isotropic films. While further experiments will be necessary—especially in regards to resolving the structural aspects—this novel material expands the pool of chiral perovskite-related materials and provides a new strategy for the use of naturally abundant

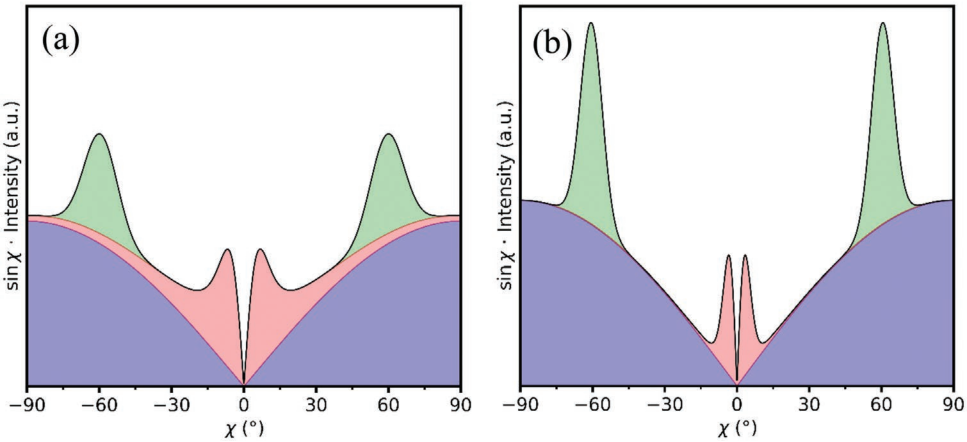

Figure 7. Pole figures derived from GIWAXS data of the (100) Bragg reflex (corresponding to $2\theta = 11.6°$ in XRD). a) The 20 s spin-coated sample displays an isotopic (blue):central (red):side (green) fractional area contribution of 0.692:0.183:0.125, and b) for the 100 s spin-coated sample possesses a corresponding fractional area contribution of 0.777:0.056:0.167, with sharper central and side intensity peaks. This difference indicates stark changes in the orientation distribution of the crystallites with spin-coating time and provides evidence for a structural explanation for the observed LDLB effect.

organic molecules as a source of chirality in applications. Further, our concept of chiral surface modification in spin-coated thin films may provide the possibility to introduce chirality into previously achiral perovskite materials without inducing major changes in terms of optoelectronic performance or the need for a complex, polymer-based matrix. Given the enormous progress in the development of high-performance perovskite-materials in recent years, this may represent a promising approach for creating bright, polarized emitters or efficient detector materials for circularly polarized light simply by adding a suitable chiral ligand to these already well-established systems.

4. Experimental Section

Materials: PbI_2 (99.999%, trace metal basis), dimethylammonium iodide (98%), dimethyl sulfoxide (≥99.9%, anhydrous), (*rac*)-3-aminobutyric acid ((*rac*)-3-ABA, 97%), and (*S*)-3-aminobutyric acid (97%) were purchased from SigmaAldrich. (*R*)-3-aminobutyric acid (>98%) was purchased from Tokyo Chemical Industry. All chemicals were used as received. Prior to use, glass substrates were cleaned with isopropanol, dried under flowing nitrogen, and treated with oxygen plasma.

Sample Preparation: (*rac*/*S*/*R*)-3-ABA functionalized $DMAPbI_3$ thin films were prepared by dissolving 0.0515 g (*rac*/*S*/*R*)-3-ABA (0.5 mmol), 0.0952 g DMAI (0.55 mmol), and 0.2305 g PbI_2 (0.5 mmol) in 1 mL DMSO by stirring the mixture at 120 °C for 1 h. Subsequently, the solution was allowed to cool down for 2 h. Thin films were then prepared by spin-coating 80 µL of the solution in question for 20 or 100 s at 6000 rpm. This was followed by a 30 min annealing step at 60 °C. $DMAPbI_3$ films were prepared in the same way but without the addition of any amino acid. Likewise, PbI_2 + (*S*/*R*)-3-ABA films were prepared without the addition of any DMAI. All samples were synthesized under an inert nitrogen atmosphere.

Dilution Series: Samples for the dilution series were produced by dissolving 0.4611 g PbI_2 (1 mmol) and 0.1903 g DMAI (1.1 mmol) in 2 mL DMSO while stirring the mixture for 45 min at 60 °C. 1 mL of the obtained solution was then added to 0.0515 g (*S*)-3-ABA. Both solutions were then stirred for an additional hour at 120 °C and subsequently left to cool down for 2 h. The solutions were then mixed in the ratios 9:1, 3:7, 1:1, 7:3, and 1:9 in order to obtain five additional precursor solutions with a volume of 200 µL each. Films were then prepared from all seven solutions by spin-coating 80 µL on glass substrates for 20 s at 6000 rpm, followed by annealing for 30 min at 60 °C. It should be noted that while this approach minimizes all variabilities that may arise from uncertainties in weighing the required amounts of PbI_2 and DMAI, 1 mL of an DMAI-PbI_2-DMSO solution contains less than half of the first solution, due to the fact that the dissolved precursors add to the overall volume, hence resulting in an overall higher concentration of the amino acid in the second solution. All samples were prepared under an inert nitrogen atmosphere.

Structural Characterization: XRD patterns were recorded using a SmartLab X-ray diffractometer (Rigaku), using Cu K_α radiation. Patterns were recorded between 2θ diffraction angles of 5° and 60°. The GISAXS/GIWAXS measurements were carried out at the Micro- and Nanofocus X-ray Scattering (MiNaXS) beamline P03 located at PETRA III (DESY, Hamburg, Germany) at a photon energy of 11.8 keV.[48] For GISAXS, the diffuse scattering signal was collected by a Pilatus 2M detector (Dectris) with a pixel size of 172×172 µm^2. For GIWAXS, the sample detector was a LAMBDA 9M detector system (pixel size 55 µm, X-Spectrum).

Optical Spectroscopy: Both CD and steady state absorption data were recorded using a J-815 CD-Spectrometer (Jasco). During measurements, the device was constantly purged with nitrogen.

For in-situ spectroscopy an Ocean Optics spectrometer (Flame) coupled with fiber optics was used to acquire the transmission measurements with an integration time of ≈0.1s per transmission spectrum. The equation $[A_\lambda = -\log_{10}(T_\lambda)]$ was used to calculate the UV–Vis absorption spectra from the transmission spectra, where A_λ is the absorbance at a certain wavelength (λ) and T_λ is the corresponding transmitted radiation. The in-situ UV–Vis transmission/absorption measurements during spin-coating were performed using a set-up described in a previous work.[49] The in-situ UV–Vis transmission/absorption measurements during thermal annealing were performed using a custom-built heating stage with a hole that allows transmission analogous to the one described in previous work.[50] In order to maximize signal intensity, the perovskite films used for these measurements were deposited on ≈150 µm thick glass substrates.

Electron Microscopy: SEM images were taken with a field emission SEM equipped with an Everhardt Thornley secondary electron detector (FEI Quanta FEG 250). An electron beam acceleration voltage of 20 kV was used.

Supporting Information

Supporting Information is available from the Wiley Online Library or from the author.

Acknowledgements

M.W.H., S.L., and F.D. acknowledge financial support from the European Research Council (ERC Starting Grant agreement no. 852084 — TWIST). M.W.H., C.M.S.-F., and F.D. recognize the support of the Bavaria California Technology Center (BaCaTec Foerderprojekt Nr 11 [2020-02]). T.K. acknowledges funding by the German Research Foundation (DFG, Grant number: KO6414). Work at the Molecular Foundry was supported by the Office of Science, Office of Basic Energy Sciences, of the U.S. Department of Energy under Contract No. DE-AC02-05CH11231. N.F. would like to express gratitude towards the Studienstiftung des Deutschen Volkes for financial support and enriching experiences. L.K.R. and P.M.-B. acknowledge funding from the Deutsche Forschungsgemeinschaft (DFG, German Research Foundation) under Germany's Excellence Strategy – EXC 2089/1 – 390776260 (e conversion). S.L. acknowledges the financial support from China Scholarship Council (CSC). F.D. and L.E. acknowledge the financial support from the Deutsche Forschungsgemeinschaft (DFG) under the Emmy Noether Program (Project 387651688). M.A. acknowledges support by the U.S. Department of Energy, Office of Science, Office of Basic Energy Sciences, Materials Sciences and Engineering Division under Contract No. DE-AC02-05-CH11231 (D2S2 program KCD2S2).

Open access funding enabled and organized by Projekt DEAL.

Conflict of Interest

The authors declare no conflict of interest.

Author Contributions

S.L. and M.W.H. performed and analyzed CD and steady state absorption measurements. T.K., M.A., and C.M.S.-F. conducted and evaluated SEM and in-situ absorption experiments. N.F. and A.K. advised on both practical and theoretical aspects of obtaining and evaluating CD results. L.K.R., C.H., S.V.R., and P.M.-B. measured and analyzed GIWAXS and GISAXS data. L.E. contributed her know-how in optical spectroscopy. I.D.S. supplied his experience on the structural characterization of perovskites. M.W.H. and F.D. conceived the general experimental design and continuously evaluated the ongoing project. M.W.H. designed the material, fabricated thin film samples, performed XRD measurements, and wrote the manuscript. The project was supervised by F.D. All authors discussed and contributed to the manuscript.

Data Availability Statement

The data that support the findings of this study are openly available in mediaTUM at https://doi.org/10.14459/2022mp1647346.

Keywords

amino acids, chiral semiconductors, chirality, chirality transfer, circular dichroism, hybrid perovskites, surface modification

Received: January 27, 2022
Revised: May 24, 2022
Published online: June 17, 2022

[1] R. Bentley, in *Encyclopedia of Molecular Cell Biology and Molecular Medicine* (Ed: R. A. Meyers), Wiley-VCH Verlag GmbH & Co. KGaA, Weinheim, Germany **2006**.
[2] Y. Yang, R. C. Da Costa, M. J. Fuchter, A. J. Campbell, *Nat. Photonics* **2013**, *7*, 634.
[3] M. Schulz, J. Zablocki, O. S. Abdullaeva, S. Brück, F. Balzer, A. Lützen, O. Arteaga, M. Schiek, *Nat. Commun.* **2018**, *9*, 2413.
[4] Y. Deng, M. Wang, Y. Zhuang, S. Liu, W. Huang, Q. Zhao, *Light: Sci. Appl.* **2021**, *10*, 76.
[5] Y.-H. Kim, Y. Zhai, H. Lu, X. Pan, C. Xiao, E. A. Gaulding, S. P. Harvey, J. J. Berry, Z. V. Vardeny, J. M. Luther, M. C. Beard, *Science* **2021**, *371*, 1129.
[6] L. Wang, Y. Xue, M. Cui, Y. Huang, H. Xu, C. Qin, J. Yang, H. Dai, M. Yuan, *Angew. Chem.* **2020**, *132*, 6504.
[7] C. Chen, L. Gao, W. Gao, C. Ge, X. Du, Z. Li, Y. Yang, G. Niu, J. Tang, *Nat. Commun.* **2019**, *10*, 1927.
[8] V. Mujica, *Nat. Chem.* **2015**, *7*, 543.
[9] G. Long, R. Sabatini, M. I. Saidaminov, G. Lakhwani, A. Rasmita, X. Liu, E. H. Sargent, W. Gao, *Nat. Rev. Mater.* **2020**, *5*, 423.
[10] M. K. Jana, R. Song, H. Liu, D. R. Khanal, S. M. Janke, R. Zhao, C. Liu, Z. V. Vardeny, V. Blum, D. B. Mitzi, *Nat. Commun.* **2020**, *11*, 4699.
[11] D. Di Nuzzo, L. Cui, J. L. Greenfield, B. Zhao, R. H. Friend, S. C. J. Meskers, *ACS Nano* **2020**, *14*, 7610.
[12] H. Lu, J. Wang, C. Xiao, X. Pan, X. Chen, R. Brunecky, J. J. Berry, K. Zhu, M. C. Beard, Z. V. Vardeny, *Sci. Adv.* **2019**, *5*, eaay0571.
[13] Y. Lu, Q. Wang, R. Chen, L. Qiao, F. Zhou, X. Yang, D. Wang, H. Cao, W. He, F. Pan, Z. Yang, C. Song, *Adv. Funct. Mater.* **2021**, *31*, 2104605.
[14] Y. Hu, F. Florio, Z. Chen, W. A. Phelan, M. A. Siegler, Z. Zhou, Y. Guo, R. Hawks, J. Jiang, J. Feng, L. Zhang, B. Wang, Y. Wang, D. Gall, E. F. Palermo, Z. Lu, X. Sun, T.-M. Lu, H. Zhou, Y. Ren, E. Wertz, R. Sundararaman, J. Shi, *Sci. Adv.* **2020**, *6*, eaay4213.
[15] C.-K. Yang, W.-N. Chen, Y.-T. Ding, J. Wang, Y. Rao, W.-Q. Liao, Y.-Y. Tang, P.-F. Li, Z.-X. Wang, R.-G. Xiong, *Adv. Mater.* **2019**, *31*, 1808088.
[16] A. Ishii, T. Miyasaka, *Sci. Adv.* **2020**, *6*, https://doi.org/10.1126/sciadv.abd3274.
[17] G. Long, C. Jiang, R. Sabatini, Z. Yang, M. Wei, L. N. Quan, Q. Liang, A. Rasmita, M. Askerka, G. Walters, X. Gong, J. Xing, X. Wen, R. Quintero-Bermudez, H. Yuan, G. Xing, X. R. Wang, D. Song, O. Voznyy, M. Zhang, S. Hoogland, W. Gao, Q. Xiong, E. H. Sargent, *Nat. Photonics* **2018**, *12*, 528.
[18] J. Ma, C. Fang, C. Chen, L. Jin, J. Wang, S. Wang, J. Tang, D. Li, *ACS Nano* **2019**, *13*, 3659.
[19] J. Ahn, E. Lee, J. Tan, W. Yang, B. Kim, J. Moon, *Mater. Horiz.* **2017**, *4*, 851.
[20] W. Chen, S. Zhang, M. Zhou, T. Zhao, X. Qin, X. Liu, M. Liu, P. Duan, *J. Phys. Chem. Lett.* **2019**, *10*, 3290.
[21] T. He, J. Li, X. Li, C. Ren, Y. Luo, F. Zhao, R. Chen, X. Lin, J. Zhang, *Appl. Phys. Lett.* **2017**, *111*, 151102.
[22] Y.-H. Kim, Y. Zhai, E. A. Gaulding, S. N. Habisreutinger, T. Moot, B. A. Rosales, H. Lu, A. Hazarika, R. Brunecky, L. M. Wheeler, J. J. Berry, M. C. Beard, J. M. Luther, *ACS Nano* **2020**, *14*, 8816.
[23] Z. N. Georgieva, B. P. Bloom, S. Ghosh, D. H. Waldeck, *Adv. Mater.* **2018**, *30*, 1800097.
[24] L. Yan, M. K. Jana, P. C. Sercel, D. B. Mitzi, W. You, *J. Am. Chem. Soc.* **2021**, *143*, 18114.
[25] C. Zhou, Y. Chu, L. Ma, Y. Zhong, C. Wang, Y. Liu, H. Zhang, B. Wang, X. Feng, X. Yu, X. Zhang, Y. Sun, X. Li, G. Zhao, *Phys. Chem. Chem. Phys.* **2020**, *22*, 17299.
[26] T. Schmitt, S. Bourelle, N. Tye, G. Soavi, A. D. Bond, S. Feldmann, B. Traore, C. Katan, J. Even, S. E. Dutton, F. Deschler, *J. Am. Chem. Soc.* **2020**, *142*, 5060.
[27] J.-T. Lin, D.-G. Chen, L.-S. Yang, T.-C. Lin, Y.-H. Liu, Y.-C. Chao, P.-T. Chou, C.-W. Chiu, *Angew. Chem.* **2021**, *133*, 21604.
[28] I. Špánik, A. Pažitná, P. Šiška, P. Szolcsányi, *Food Chem.* **2014**, *158*, 497.

[29] V. Y. Sirenko, O. I. Kucheriv, D. D. Naumova, I. V. Fesych, R. P. Linnik, I.-A. Dascălu, S. Shova, I. O. Fritsky, I. A. Gural'skiy, *New J. Chem.* **2021**, *45*, 12606.
[30] D. Thevenet, V. Pastor, I. Baccelli, A. Balmer, A. Vallat, R. Neier, G. Glauser, B. Mauch-Mani, *New Phytol.* **2017**, *213*, 552.
[31] D. Ju, T. Zhao, D. Yangyang, G. Zhang, X. Hu, D. Cui, X. Tao, *J. Mater. Chem. A* **2017**, *5*, 21919.
[32] Y. Wang, Y. Liu, Y. Wu, J. Jiang, C. Liu, W. Liu, K. Gao, H. Cai, X. S. Wu, *CrystEngComm* **2020**, *22*, 7090.
[33] T. Yamaguchi, T. Kimura, H. Matsuda, T. Aida, *Angew. Chem., Int. Ed.* **2004**, *43*, 6350.
[34] J. Schlipf, P. Müller-Buschbaum, *Adv. Energy Mater.* **2017**, *7*, 1700131.
[35] H. Wang, Y. Liu, J. Yu, Y. Luo, L. Wang, T. Yang, B. Raktani, H. Lee, *ACS Appl. Mater. Interfaces* **2022**, *14*, 3559.
[36] M. Jakob, A. von Weber, A. Kartouzian, U. Heiz, *Phys. Chem. Chem. Phys.* **2018**, *20*, 20347.
[37] J. Schlipf, P. Docampo, C. J. Schaffer, V. Körstgens, L. Bießmann, F. Hanusch, N. Giesbrecht, S. Bernstorff, T. Bein, P. Müller-Buschbaum, *J. Phys. Chem. Lett.* **2015**, *6*, 1265.
[38] T.-B. Song, Z. Yuan, F. Babbe, D. P. Nenon, E. Aydin, S. de Wolf, C. M. Sutter-Fella, *ACS Appl. Energy Mater.* **2020**, *3*, 2386.
[39] G. Albano, F. Salerno, L. Portus, W. Porzio, L. A. Aronica, L. Di Bari, *ChemNanoMat* **2018**, *4*, 1059.
[40] A. Forde, D. Ghosh, D. Kilin, A. C. Evans, S. Tretiak, A. J. Neukirch, *J. Phys. Chem. Lett.* **2022**, *13*, 686.
[41] Y. Shindo, *Appl. Spectrosc.* **1985**, *39*, 713.
[42] Y. Shindo, M. Nakagawa, *Rev. Sci. Instrum.* **1985**, *56*, 32.
[43] G. Albano, G. Pescitelli, L. Di Bari, *Chem. Rev.* **2020**, *120*, 10145.
[44] A. von Weber, D. C. Hooper, M. Jakob, V. K. Valev, A. Kartouzian, U. Heiz, *ChemPhysChem* **2019**, *20*, 62.
[45] R. Wolfe, V. J. Fratello, M. McGlashan-Powell, *J. Appl. Phys.* **1988**, *63*, 3099.
[46] M. T. Sirtl, M. Armer, L. K. Reb, R. Hooijer, P. Dörflinger, M. A. Scheel, K. Tvingstedt, P. Rieder, N. Glück, P. Pandit, S. V. Roth, P. Müller-Buschbaum, V. Dyakonov, T. Bein, *ACS Appl. Energy Mater.* **2020**, *3*, 11597.
[47] S. Tu, T. Tian, A. Lena Oechsle, S. Yin, X. Jiang, W. Cao, N. Li, M. A. Scheel, L. K. Reb, S. Hou, A. S. Bandarenka, M. Schwartzkopf, S. V. Roth, P. Müller-Buschbaum, *Chem. Eng. J.* **2022**, *429*, 132295.
[48] A. Buffet, A. Rothkirch, R. Döhrmann, V. Körstgens, M. M. Abul Kashem, J. Perlich, G. Herzog, M. Schwartzkopf, R. Gehrke, P. Müller-Buschbaum, S. V. Roth, *J. Synchrotron Radiat.* **2012**, *19*, 647.
[49] M. Abdelsamie, K. Zhao, M. R. Niazi, K. W. Chou, A. Amassian, *J. Mater. Chem. C* **2014**, *2*, 3373.
[50] K. Wang, R.-Z. Liang, J. Wolf, Q. Saleem, M. Babics, P. Wucher, M. Abdelsamie, A. Amassian, M. R. Hansen, P. M. Beaujuge, *Adv. Funct. Mater.* **2016**, *26*, 7103.